Molecular Catalysis 515 (2021) 111911

Contents lists available at ScienceDirect

Molecular Catalysis

journal homepage: www.journals.elsevier.com/molecular-catalysis

Effect of Ru loading on Ru/CeO_2 catalysts for CO_2 methanation

Sergio López-Rodríguez [a], Arantxa Davó-Quiñonero [a,b], Esther Bailón-García [a], Dolores Lozano-Castelló [a], Agustín Bueno-López [a,*]

[a] Inorganic Chemistry Department, University of Alicante, Carrertera de San Vicente del Raspeig s/n E-03080, Alicante, Spain
[b] School of Chemistry, CRANN and AMBER Research Centres, Trinity College Dublin, College Green, Dublin, Ireland

ARTICLE INFO

Keywords:
CO_2 methanation
CO_2 hydrogenation
Ru/CeO_2
DRIFTS
CO_2 valorisation

ABSTRACT

The conversion of CO_2 towards added valuable products is considered as a potential alternative to achieve the increase of the petrochemical industry while reducing the CO_2 emissions. In the present work, the effect of Ru loading on CeO_2 supports has been studied for the CO_2 methanation reaction, and catalysts with different Ru loading in the 1–5 wt. % range have been prepared, characterized, and tested. The optimum Ru loading has been found to be 2.5 wt. %. Ruthenium cations are reduced at the lowest temperature for this optimum loading according to H_2-TPR experiments (even at room temperature), and the highest proportion of ruthenium cations with strong interaction with ceria is achieved, as deduced from XPS. XRD characterization suggests partial insertion of ruthenium cations into the ceria lattice.

In situ DRIFTS experiments evidenced that the balance between formation upon CO_2 chemisorption and further hydrogenation of surface carbon intermediates is optimum for 2.5 wt. % Ru/CeO_2. For low metal contents, the CO_2 chemisorption is limited and no relevant, while as the metal content is increased, the hydrogenation of carbon species is less favourable. The 2.5 wt.% Ru/CeO_2 catalyst comprises a balance between surface-carbon groups formation and further hydrogenation.

1. Introduction

Reducing the CO_2 emissions from fossil fuels to mitigate the climate change is mandatory to achieve the 80–95% of reduction by 2050 [1,2]. In 2020, the global greenhouse emissions were sharply decreased by 2.3 billion of tonnes because of the COVID-19 pandemic impacted over economy and society, reducing the weekly global warming emissions as lockdowns started to be imposed in the main greenhouse emitters [3]. Despite this decline was insufficient, and the emissions in 2021 are rebounding to pre-COVID levels, a rapid green deployment of recovery planning are emerging in order to boost the economic growth and reduce the emissions simultaneously.[4] In this scenario, efforts must be made to scaling up technologies which provide successful transitions from carbon to renewable fuels. To do so, circular economy is laying the foundations for the next strategic production system provided by the key competent organisms and the use of CO_2 as feedstocks, combined with large hydrogen production plants, could supply the increasing of the commodities demand on the roadmap to 2050 while meeting the emission targets [5–11].

The CO_2 methanation reaction (Eq. (1)) comprises the C1 chemistry within the heterogeneous catalysis and has been extensively studied due to the practical implementation in the current power and petrochemical plants.

$$CO_2 + H_2 \rightarrow CH_4 + H_2O \ \Delta H^0 = -164 \ kJ \bullet mol^{-1} \quad (1)$$

The reaction is carried out in gas phase in the presence of a catalyst due to the strong kinetic limitations. It is generally accepted that nickel and ruthenium as active phases show high activity and selectivity within a range of operating temperatures that vary from 200–250 °C for ruthenium to 350–400 °C for nickel, despite other reports show high performances with noble metal such as Rh and Pt [12–14]. In these heterogeneous catalysts, the CO_2 dissociation and hydrogenation steps occur onto the metal sites. However, bifunctional catalysts are avowed to be highly efficient due to the synergistic effects between the metal sites and the support. The hydrogenation steps take place over reduced metal sites and the activation of CO_2 can occur onto either a partially reduced support or onto the reduced metal sites.

According to the literature, it is well described that reducible supports such as TiO_2, ZrO_2, CeO_2-based catalysts exhibit higher catalytic activities than inert supports such as Al_2O_3 or SiO_2 [15–23]. This is due

* Corresponding author.
E-mail address: agus@ua.es (A. Bueno-López).

https://doi.org/10.1016/j.mcat.2021.111911
Received 7 August 2021; Received in revised form 1 September 2021; Accepted 16 September 2021
Available online 28 September 2021

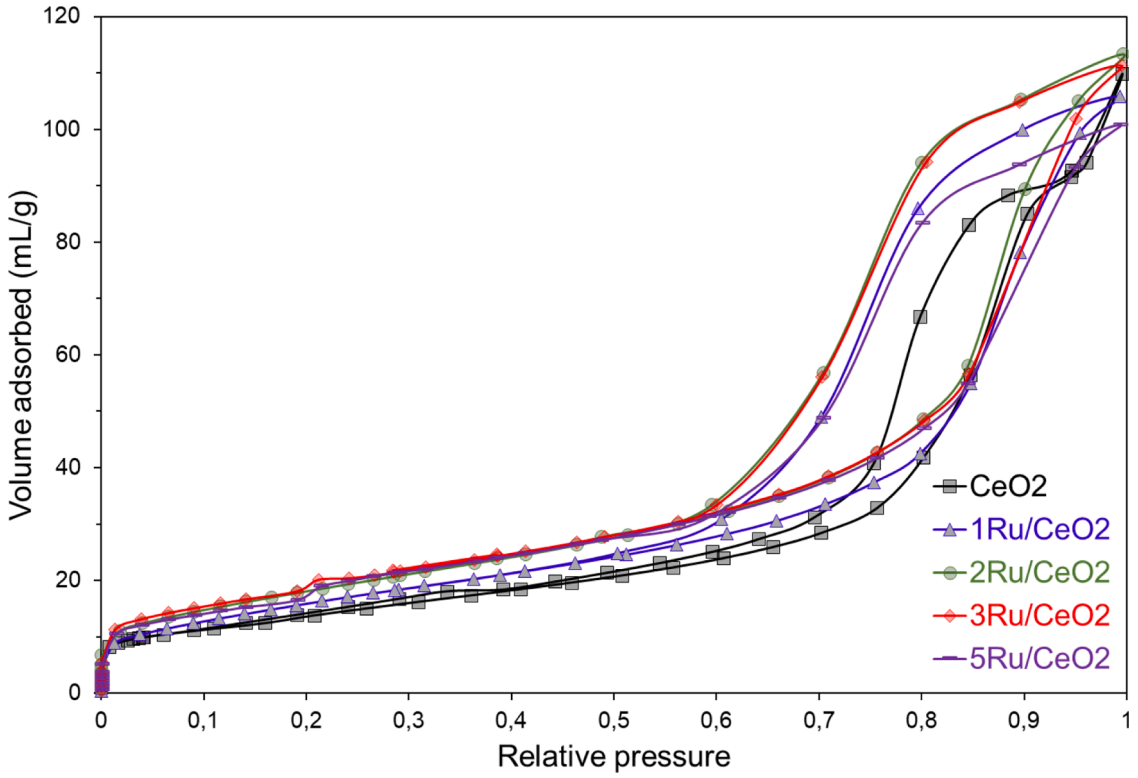

Fig. 1. N_2 adsorption-desorption isotherms of fresh catalysts at -196 °C after outgassing at 250 °C for 4h.

to their ability to activate the CO_2 molecules onto the support, in which the metal/support interface and the oxygen vacancies usually play a critical role in the catalytic performance and in the reaction mechanism. As such, two active centres are responsible for the CO_2 conversion towards CH_4 rather than one [24–27].

It is deeply studied that Ni/CeO_2 and Ru/CeO_2 catalysts formulations outperform their counterparts in activity, stability, and selectivity [18,20,22,28–35]. The high oxygen storage capacity and oxygen mobility of ceria activate the CO_2 molecules onto the surface oxygen vacancies even at low temperatures, and the creation of these effective active sites depends on the metal-support interactions [24,26,27,35–40]. This process leads to the creation of reaction intermediates that can be active or just spectators through the reaction mechanism which is still under debate. The reaction mechanism is claimed to be carried out either by an associative reaction path or by a dissociative reaction path, and it has been reported that the catalytic surface is covered by ruthenium-monocarbonyls, ruthenium-multicarbonyls, carbonates, formates, bicarbonates and/or isolate hydroxyls among other species during the reaction [41–46]. The stability of such intermediates is influenced by the nature and the morphology of the active centres (particle size, strong metal-support interactions, surface areas), and the reactivity towards high conversion and selectivity is affected by the role of these intermediates [22,24,36,47–49].

In spite of Ru/CeO_2 catalysts have been studied in a relevant number of articles, the effect of the Ru loading needs to be analysed in more detail, [50–53] and the goal of this study is to investigate the CO_2 hydrogenation to CH_4 over Ru/CeO_2 catalysts by varying the metal loading from 1 wt.% up to 5 wt.%, seeking an optimum content which comprises the Ru-CeO_2 interaction and combines efficient CO_2 chemisorption which further hydrogenation of the reaction intermediates.

2. Experimental details

2.1. Catalyst preparation

Ceria-supported ruthenium catalysts were prepared by wet impregnation method. Cerium oxide was obtained by calcination of Ce $(NO_3)_2 \bullet 6H_2O$ (Alfa Aesar, 99.5%) in static air at 600 °C for 6 h. The required amount of Ruthenium (III) acetylacetonate (Sigma-Aldrich, 97%) was dissolved in toluene and loaded onto the support in order to obtain formulations with different target contents (1, 2, 3 and 5 wt. %). Finally, the catalysts were dried at 110 °C overnight and thermal treated at 350 °C for 3 h in N_2 atmosphere. The catalysts are labelled as $1Ru/CeO_2$, $2Ru/CeO_2$, $3Ru/CeO_2$ and $5Ru/CeO_2$, respectively. Note that the catalysts nomenclature includes the target ruthenium loading, but not the actual loading determined by ICP in order to avoid decimals in the nomenclature.

2.2. Catalyst characterization

The textural properties of catalysts were determined by N_2 physisorption isotherms measured at –196 °C in an Autosorb-6 device (Quantachrome) after outgassing each catalyst at 250 °C for 4h under vacuum conditions.

The crystallographic properties were analysed by X-Ray diffraction in a Rigaku Miniflex II diffractometer. The diffractograms were recorded in a range of 2θ from 20 ° to 90 °, with a step of 0.025 °. The wavelength used was $\lambda = 0.155418$ nm corresponding to the CuKα radiation. The average crystal size of ceria was determined using the Scherrer equation [54,55].

The ruthenium content was determined by ICP-OES in a Perkin Elmer device (Optima model 4300 DV) after catalyst digestion in a HCl/HNO_3 solution (3:1 volume) assisted by microwaves.

The reducibility of the catalysts was examined by H_2-TPR (Temperature Programmed Reduction) in a Micromeritics Pulse Chemisorb 2705 device. 25 mg of catalyst was placed in a tubular quartz reactor coupled

Table 1
Textural and structural properties of the Ru/CeO_2 catalysts.

Sample	Ru content (w%)	BET (m^2/g)	Cell parameter (nm)	Crystallite size (nm)
CeO_2	-	50	0.5423	14
$1Ru/CeO_2$	0.97	58	0.5427	14
$2Ru/CeO_2$	1.65	64	0.5418	14
$3Ru/CeO_2$	2.54	66	0.5418	13
$5Ru/CeO_2$	4.10	68	0.5400	13

with a TCD detector and heated at 10 °C/min up to 950 °C under a mixture of 5%H_2/Ar with 40 mL/min total flow. The amount of H_2 consumed in the H_2-TPR experiments has been quantified using CuO as reference material.

The surface of the catalysts was studied by X-ray photoelectron spectroscopy (XPS) performed in a K-ALPHA Thermo Scientific device. Al-Kα radiation (1486.6 eV) was used as X-ray source and C1s transition at 284.6 eV was used as internal reference to adjust the binding energy scale.

2.3. Catalytic tests

The catalytic activity was measured in a fixed-bed tubular reactor (10 mm inner diameter) containing 100 mg of catalyst mixed with SiC particles (1 – 1.25 mm) to reach a bed volume of 1 cm^3. The catalysts were pre-treated in situ at 500 °C for 1 h under 100 mL/min of a 50% vol. H_2/He mixture. After cooling down to room temperature, 100 mL/min of a methanation mixture consisting of 10% vol. CO_2, 40% vol. H_2 and He balance was fed to the reactor at 1 atm. The temperature was increased up to 400 °C in steps of 20 °C while the outlet gas composition was analysed under steady state conditions by a gas chromatograph (Agilent 8860 GC System) equipped with two pack columns (Porapak Q80/100 and Molecular Sieve 13X) coupled to a TCD detector.

2.4. In situ DRIFTS experiments

In situ DRIFTS experiments were performed in a Jasco infrared spectrometer, model FT/IR-4000, using a reaction cell with temperature and gas flow control. Spectra were recorded from 4000 cm^{-1} to 1000 cm^{-1} in steps of 1cm^{-1}. The catalyst was mixed with KBr in a 1/50 ratio.

The catalysts were pretreated in situ at 400 °C for 1 hour under 50 % vol. H_2/He gas flow. Then, the reaction cell was cooled down in H_2/He to room temperature, and a background spectrum was recorded in these conditions, which was subtracted to further spectra. Then, a gas mixture with 10 % vol. CO_2 in He was fed to the cell (100 mL/min), and a spectrum was recorded once the steady state was achieved. The system was purged with He for 15 minutes afterwards, and then a gas mixture with 40% vol. H_2 in He was fed (100 mL/min). A new spectrum was recorded in steady state conditions, and He was used again to purge the system for 15 min afterwards. This protocol described for 25 °C was repeated at 100, 200, 300 and 400 °C.

3. Results and discussion

3.1. Catalyst characterization

The specific surface area of the catalysts was determined form the N_2 adsorption-desorption isotherms recorded at –196 °C, which are included in Fig. 1. The isotherms shape evidence low microporosity for all catalysts, as expected, and presence of mesopores is deduced from the hysteresis loop. The BET specific surface areas, included in the Table 1, range between 50 and 68 m^2/g, being consistent with values reported on literature for this type of material [17,19,30,47,56,57]. The small increase of the BET surface area upon Ru impregnation and further thermal treatment is tentatively attributed to changes on the ceria surface that make certain inter-particle space available for N_2 adsorption.

The X-ray diffractograms are shown in Fig. 2, and both the cell parameter and crystallite size were determined and compiled in Table 1. All diffractograms show the characteristic peaks of fluorite, which is the structure of CeO_2, with the main peaks located at 28.5, 33.1, 47.6 and 56.5 ° (JCPDS file 34-0394). Segregated ruthenium phases are not observed, which indicates that ruthenium oxide species are highly dispersed on ceria support, or that the particle size of such species is small. The crystallite size of fluorite ceria is 13–14 nm for all catalysts,

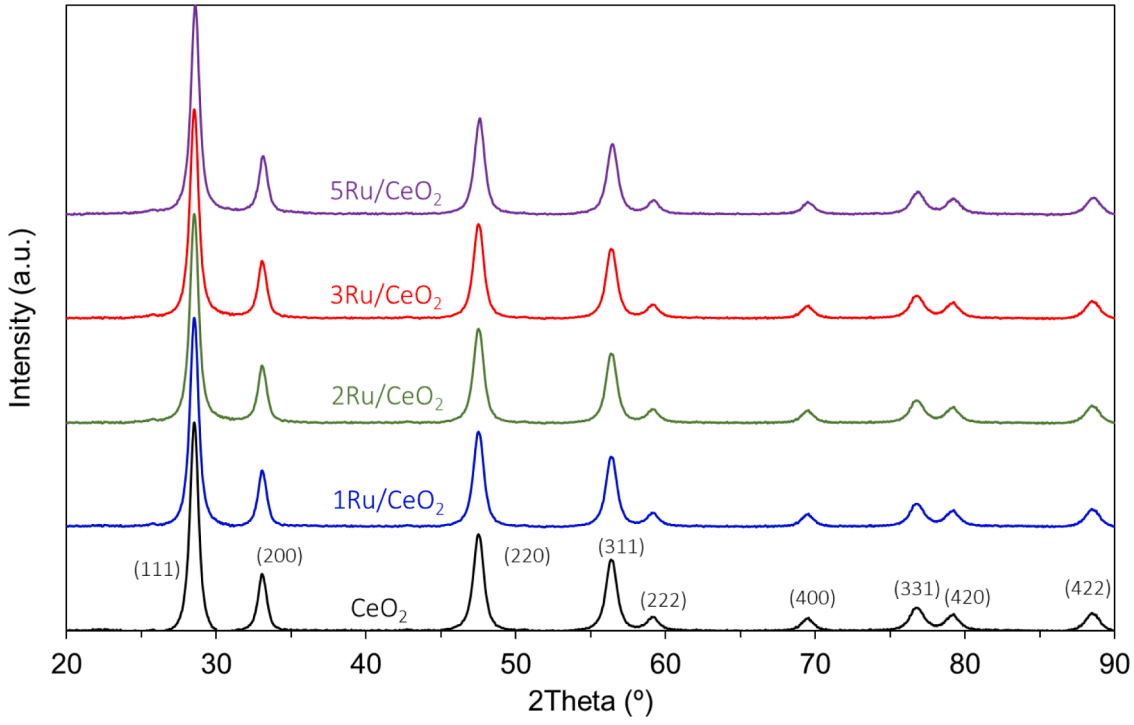

Fig. 2. X-Ray diffractograms of fresh catalysts.

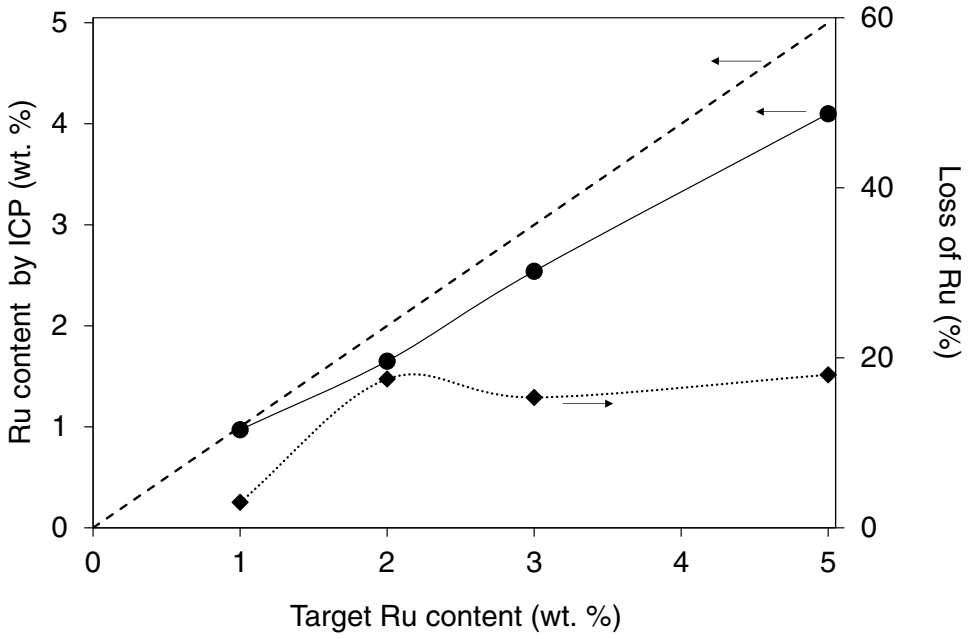

Fig. 3. Ru content on the catalysts measured by ICP and percentage of Ru loss compared to the nominal Ru loading.

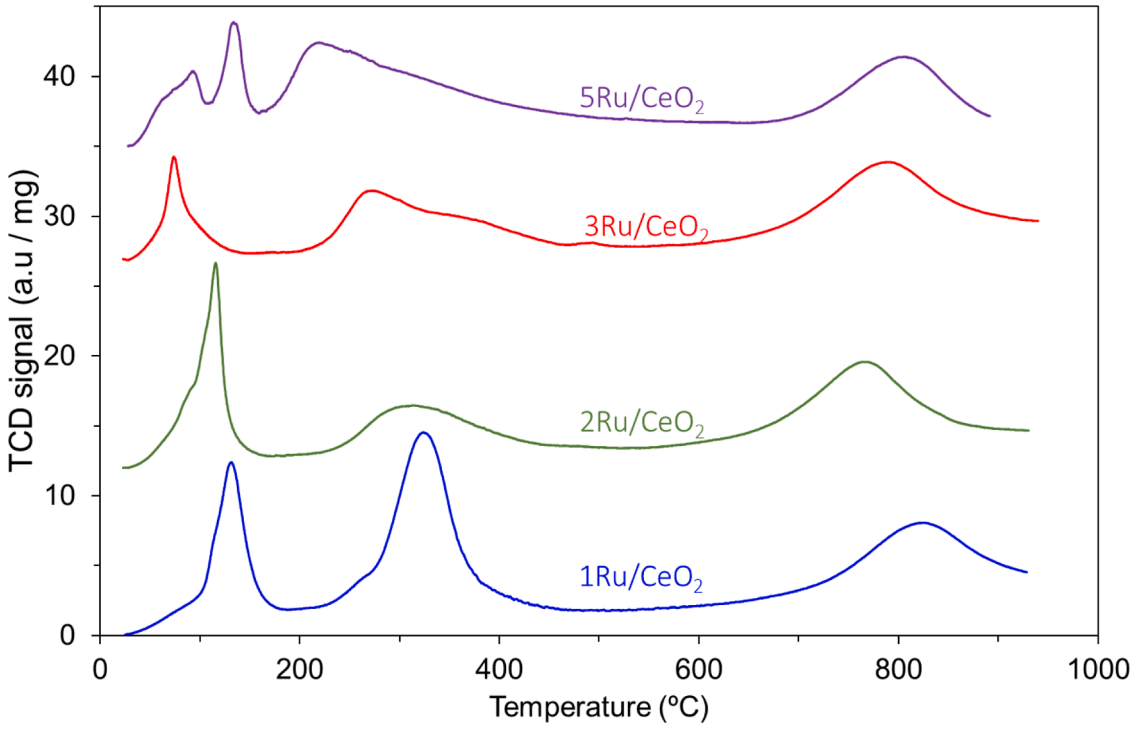

Fig. 4. H_2-TPR profiles for the Ru/CeO_2 catalysts.

and this is the expected size according to the specific surface areas of the catalysts. The lattice parameter of all catalysts is around the value measured for bare ceria (0.5423 nm), but slightly decreasing with the ruthenium content. This could suggest that ruthenium is being incorporated into the ceria lattice at least partially.

The ruthenium content loaded on the catalysts was determined by ICP, and the obtained values are included in Table 1 and plotted in Fig. 3 against the target loading.

The amount of Ru determined by ICP is slightly lower to the target value for all catalysts, as expected, since ruthenium is known to form volatile oxides that can be released during the thermal treatment [58] For this reason, the thermal treatment was carried out in inert atmosphere to minimize this effect, but RuO_x species can still be formed with oxygen available on the solid phases. It is also known that CeO_2 interacts strongly and stabilizes RuO_x species, [59,60]. diminishing the release of volatile ruthenium oxides regarding other metal oxide supports. Fig. 3 indicates that the amount of Ru lost by the $1Ru/CeO_2$ catalyst is significantly low, in agreement with the stabilizing effect of CeO_2. However, for higher Ru target loading the loss of Ru is near 20 % in all cases.

Table 2
Quantitative estimations determined from the H_2-TPR experiments.

Sample	Low Temperature (below 180 °C) mmol H_2/mmol Ru	Mild Temperature (180-600 °C) mmol H_2/mmol Ce	High Temperature (above 600 °C) mmol H_2/mmol Ce
1Ru/CeO_2	2.75	0.11	0.05
2Ru/CeO_2	2.33	0.05	0.07
3Ru/CeO_2	0.80	0.06	0.07
5Ru/CeO_2	1.93	0.09	0.05

The amount of Ru loaded on the catalysts strongly affects the H_2 reduction, as it is deduced from the temperature programmed reduction profiles included in Fig. 4.

Three temperature ranges can be distinguished in the H_2-TPR profiles: below 180 °C (low temperature), between 180 and 600 °C (mild temperature) and above 600 °C (high temperature). The amount of H_2 consumed in these three regions has been quantified for each catalyst, and the values have been included in Table 2.

According to Fig. 4, RuO_x species are reduced below 180 °C, and the H_2 mole consumption in this low temperature region depends on the Ru loading. The position of the low temperature peak decreases by increasing the Ru loading from 1% to 3%, evidencing that the higher the ruthenium loading the greater the reducibility. However, this trend is not followed by 5Ru/CeO_2, and the reducibility of the Ru species is worse in this case than in 3Ru/CeO_2, that is, the reducibility of the cationic species of ruthenium reaches an optimum for 3Ru/CeO_2.

The amounts of H_2 consumed below 180 °C (see Table 2) are consistent with this conclusion. According to previous reports, it is reasonable to expect that ruthenium is mainly forming Ru^{4+} species in this type of catalysts [61–65], and the stoichiometry of the Ru^{4+} reduction to Ru^0 predicts a H_2/Ru mole ratio of 2. The mmol H_2/mmol Ru calculated and included in Table 2 are higher than 2 for low Ru loading catalysts (1Ru/CeO_2 and 2Ru/CeO_2), suggesting that some surface Ce^{4+} cations are being reduced to Ce^{3+} together with Ru^{4+} reduction, and near 2 for 5Ru/CeO_2. On the contrary, the amount of H_2 consumed by 3Ru/CeO_2 is only 0.8 because RuO_x species are partially reduced even at room temperature before start heating (see below in the XPS discussion).

Note that the H_2 reduction profiles below 180 °C show peaks with shoulders or double peaks, evidencing the presence of different types of cationic species of ruthenium. This is particularly evident for the catalyst with the highest Ru loading (5Ru/CeO_2). The presence of different species of ruthenium is in accordance with the XRD conclusions, that is, part of the ruthenium is being inserted into the CeO_2 lattice and part is forming segregated RuO_x oxides, probably RuO_2.

The consumption of H_2 in the 180–600 °C range is attributed to the surface reduction of Ce^{4+} cations to Ce^{3+}. The maximum of this mild temperature peak decreases by increasing the Ru loading because ruthenium, once reduced to Ru^0, enhances H_2 dissociation catalysing the surface reduction of ceria, and the higher the ruthenium loading the higher the catalytic effect.

On the contrary, the reduction of bulk ceria, which occurs above 600 °C, suffers little effect of the ruthenium loading because ruthenium is mainly located on the ceria particles surface, even the fraction of

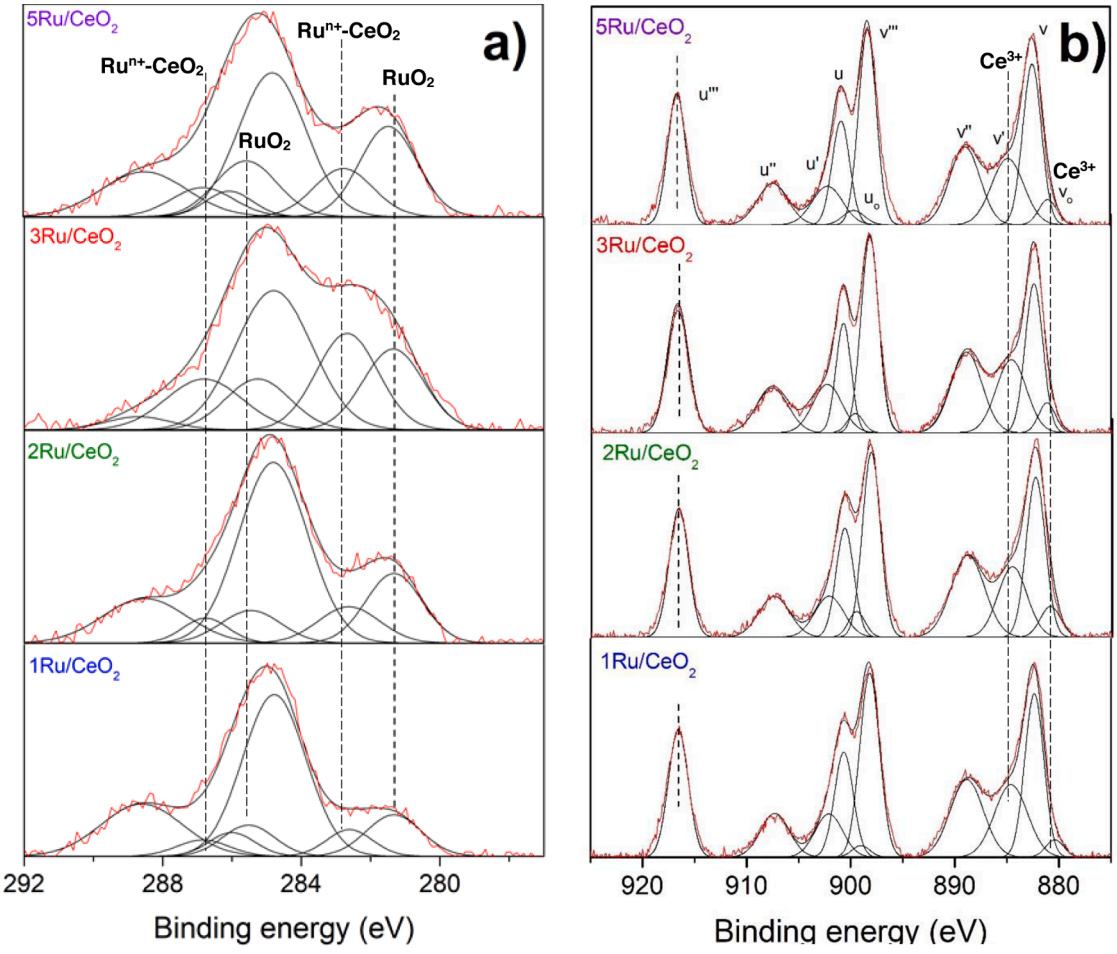

Fig. 5. XPS spectra for (a) Ru3d and (b) Ce3d core level regions.

Table 3
Relative percentages obtained from XPS Ru3d and Ce3d core level spectra.

Sample	RuO_2 (%)	Ru^{n+}-CeO_2 (%)	Ce^{3+} (%)*
$1Ru/CeO_2$	65	35	22
$2Ru/CeO_2$	64	36	22
$3Ru/CeO_2$	45	55	24
$5Ru/CeO_2$	65	35	22

* Ce^{3+} percentage with regard to total $Ce^{3+} + Ce^{4+}$.

ruthenium doping the ceria lattice.

As a summary, the H_2-TPR experiments evidence that the Ru loading affects the reduction of the Ru cations and the reduction of surface Ce^{4+} cations, while not significantly bulk ceria cations reduction. The reducibility of Ru species is best for $3Ru/CeO_2$, and for low Ru loading surface ceria cations are reduced together with those of ruthenium below 180 °C. In addition, the amount of Ru strongly affects the massive reduction of surface ceria above 180 °C, the higher the Ru loading the easier the surface ceria reduction.

Additional information about the nature of the surface ruthenium species is obtained by XPS characterization. Fig. 5 shows the spectra in the Ru3d energy region together with those of Ce3d.

The analysis of the Ru3d region is complex because the Ru contributions partially overlap with those of C1s, and the spectra must be deconvoluted taking both C1s and Ru3d events into account. Four peaks can be attributed to ruthenium, two of them in the $Ru3d_{5/2}$ region (below 284 eV) and two in the $Ru3d_{3/2}$ region (above 284 eV) [64], and the remaining peaks observed in Fig. 5a are assigned to carbon. The presence of two Ru peaks in each region indicates the formation of two ruthenium species, in accordance with the conclusions of H_2-TPR and XRD characterization. The energies of the Ru peaks at 281.2 eV and 282.5 eV are consistent with the presence of cationic ruthenium species, since the metallic Ru 3d5/2 peak is reported to appear around 280 eV [64]. The peak at 281.2 eV can be assigned to RuO_2, and the peak at 282.5 eV evidences the presence of cationic species of ruthenium with higher positive charge density, as expected for Ru^{n+} cations inserted into the ceria lattice, again in accordance with XRD observations.

The areas under the RuO_2 and Ru^{n+}-CeO_2 peaks have been quantified and expressed in percentage (Table 3), in order to estimate the proportion of RuO_2 and ruthenium cations with strong interaction with ceria.

The proportion of both species of ruthenium are similar for all catalysts (65 % RuO_2 and 35 % of Ru^{n+} species with strong interaction with ceria), except for the $3Ru/CeO_2$ catalyst where the proportion of ruthenium species with strong interaction with ceria increases to 55% of the total ruthenium observed by XPS. This catalyst showed the reducibility of the ruthenium cations at the lowest temperature in the H_2-TPR experiments (Fig. 4), and as it will be shown in the next section, is also the most active catalyst for CO_2 methanation. However, the percentage of Ce^{3+} cations with regard to total $Ce^{3+} + Ce^{4+}$ cations is quite similar for all catalysts (22–24%).

3.2. CO_2 methanation catalytic tests

CO_2 methanation catalytic experiments were performed with the ruthenium catalysts in a fixed-bed reactor, and Fig. 6 shows the CO_2 conversion results obtained in these experiments. As expected, all Ru/CeO_2 catalysts are active for CO_2 methanation, with 100 % selectivity to CH_4 in all cases regardless the reaction temperature. The shape of all CO_2 conversion curves is qualitatively similar, increasing with temperature above the onset until reaching the thermodynamic equilibrium. However, the ruthenium loading strongly affects the reaction onset and the dependence of conversion with temperature, the $3Ru/CeO_2$ catalyst being the most active one. Aligned with this, high conversion towards CH_4 at low temperatures remarks these CeO_2-based formulations as potential catalysts compared with other inert supports, as it was previously described on the section above.

The inset in Fig. 6 plots the temperature for 50 % CO_2 conversion as a function of the Ru loading on the catalysts determined by ICP, where it is observed that this temperature decreases by increasing the ruthenium

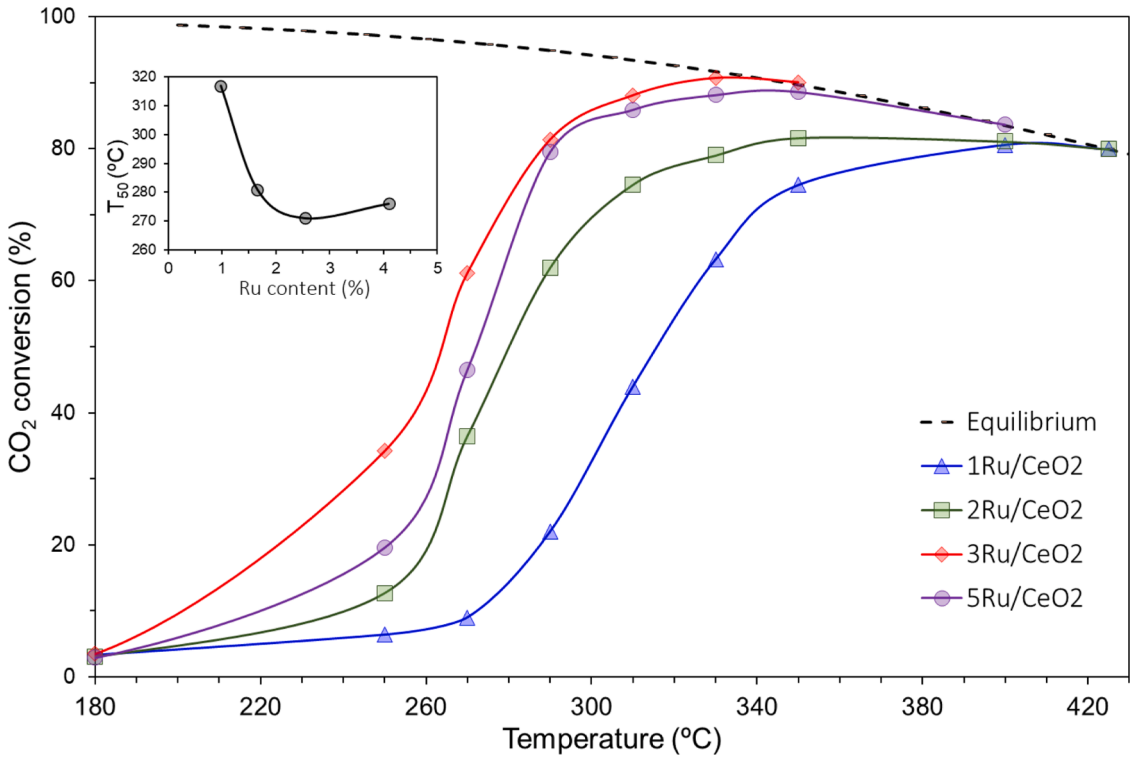

Fig. 6. CO_2 methanation tests performed in a fixed-bed reactor under steady state conditions. Reduction pre-treatment at 500 °C for 1 h under 50 % vol. H_2/He. Reaction conditions at 10% vol. CO_2, 40% vol. H_2 with He balance.

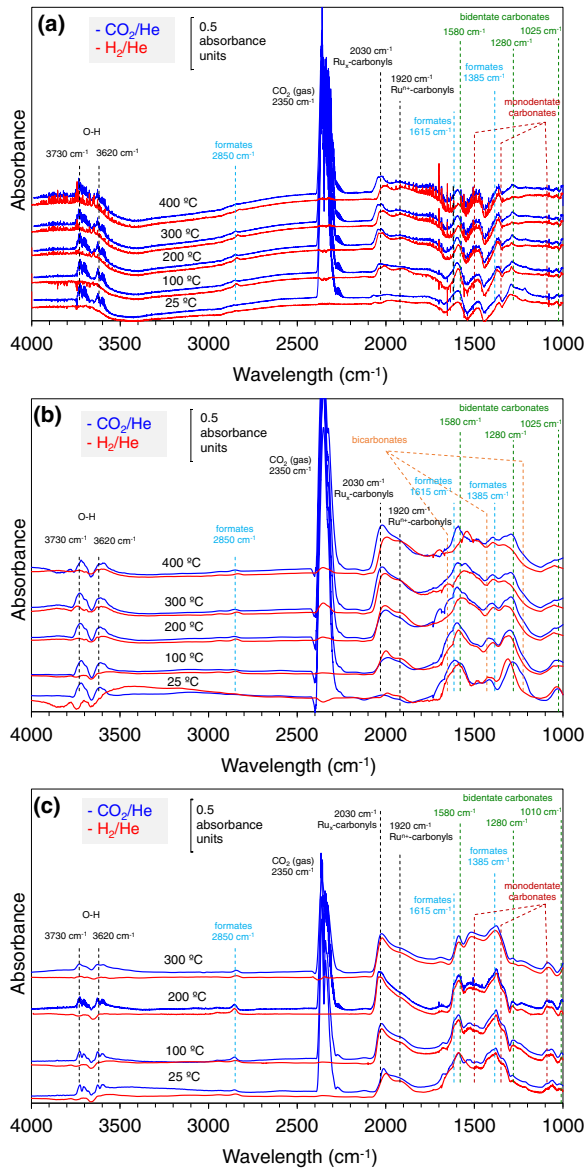

Fig. 7. In situ DRIFT experiments performed under CO_2/He and H_2/He at different temperatures after catalysts reduction at 400 °C for 1 h in H_2/He. (a) 1Ru/CeO_2, (b) 3Ru/CeO_2 and (c) 5Ru/CeO_2.

loading from 1Ru/CeO_2 to 3Ru/CeO_2, whiles higher Ru loading has a negative effect in the conversion.

These catalytic results are consistent with previous characterization, and the most active catalyst (3Ru/CeO_2) is the catalyst where ruthenium cations are reduced at the lowest temperature (according to H_2-TPR experiments) and is also the catalyst with the highest proportion of ruthenium cations with strong interaction with ceria (as deduced from XPS). It was previously reported [47], that the rate limiting step of the CO_2 methanation using Ru/CeO_2 catalysts is the hydrogenation of surface carbon intermediates created on the catalyst surface upon CO_2 chemisorption, and optimization of the Ru loading seems to be critical to optimise the hydrogenation of the reaction intermediates.

3.3. *In situ DRIFTS experiments*

The species created on the catalysts surface upon CO_2 chemisorption and their depletion by H_2 reduction were studied by *in situ* DRIFT spectroscopy. The catalysts were pretreated in situ under H_2/He, and after cooling, the gas was switched to CO_2/He first and to H_2/He afterwards at different temperatures from 25 to 400 °C. Fig. 7 shows the spectra recorded under CO_2/He and H_2/He for 1Ru/CeO_2, 3Ru/CeO_2 and 5Ru/CeO_2. The spectra show bands that are consistent with the presence of bidentate carbonates (1580, 1280 and 1025 cm^{-1}), monodentate carbonates (1500, 1350 and 1090 cm^{-1}), bicarbonates (1225, 1430, 1650 and ~3600-3700 cm^{-1}), formates (2850, 1615 and 1385 cm^{-1}) and ruthenium carbonyls (1920 and 2030 cm^{-1}).

These bands are in accordance with the associative chemisorption of CO_2, yielding carbonates and/or bicarbonates, and with the dissociative chemisorption yielding ruthenium carbonyls. The presence of formates evidences partial hydrogenation of the chemisorbed CO_2 with hydrogen available on the catalyst surface, even occurring at room temperature. The bands at 3730 and 3620 cm^{-1} are most likely CO_2 overtones, since they are observed under CO_2/He and disappear after switching to H_2/He [66]. This region typically shows O-H stretching bands, but note that a background spectrum was recorded after the reduction with H_2/He and was subtracted to all spectra. The surface of ceria is expected to be highly hydroxylated in these conditions but the O-H bands are not observed because of the background subtraction.

The DRIFTS bands intensity is lowest for the lowest ruthenium loading catalyst (1Ru/CeO_2), being much more intense for 3Ru/CeO_2 and 5Ru/CeO_2. This indicates that the CO_2 chemisorption capacity of 1Ru/CeO_2 is poor in comparison to catalysts with higher ruthenium loading, and this could be one of the reasons of the lowest CO_2 methanation activity observed in catalytic tests (Fig. 6) for 1Ru/CeO_2.

Bands compatible with the formation of bicarbonates, bidentate carbonates, formates and ruthenium carbonyls are observed on 3Ru/CeO_2 spectra recorded in CO_2/He, and switching the gas from CO_2/He to H_2/He leads to the intensity decrease of certain bands.

The 5Ru/CeO_2 spectra recorded in CO_2/He are compatible with the presence of monodentate and bidentate carbonates, formates and ruthenium carbonyls. The main difference between 5Ru/CeO_2 and 3Ru/CeO_2 spectra is the formation of monodentate carbonates on 5Ru/CeO_2 while bicarbonates on 3Ru/CeO_2. In addition, the intensity of the signals obtained with 5Ru/CeO_2 do not change significantly after switching CO_2/He to H_2/He, that is, hydrogenation of chemisorbed CO_2 species seems to be more favourable for 3Ru/CeO_2 than for 5Ru/CeO_2.

A more detailed analysis of changes in the surface species during the DRIFTS experiments has been carried out, and the intensity of selected bands has been plotted in Fig. 8 as a function of temperature for formates (1615 cm^{-1}), bidentate carbonates (1280 cm^{-1}), Ru_x carbonyls (2030 cm^{-1}) and Ru^{n+} carbonyls (1920 cm^{-1}).

Formates band intensity (Fig. 8a) is highest for the 3Ru/CeO_2 catalyst under CO_2/He, and decreases in H_2/He suggesting that formates are reaction intermediates in this case. Bicarbonates (Fig. 8b) on 3Ru/CeO_2 are also slightly removed in H_2/He, but in much lesser extent than formates. On the contrary, the intensity of formates band of 5Ru/CeO_2 (Fig. 8a) does not change after switching from CO_2/He to H_2/He, evidencing that hydrogenation of 3Ru/CeO_2 formates is more favourable than hydrogenation of 5Ru/CeO_2 formates. Formates band of 1Ru/CeO_2 shows the lowest intensity and neither change after switching from CO_2/He to H_2/He.

The intensity of carbonyl bands (Ru_x-carbonyls in Fig. 8c and Ru^{n+}-carbonyls in Fig. 8d) strongly depends on the Ru loading, and as a general trend, increases with temperature until steady values. The lowest intensity is achieved by 1Ru/CeO_2, as expected, and at low temperature highest values are reached by 5Ru/CeO_2. However, 3Ru/CeO_2 Ru_x-carbonyls intensity increases significantly with temperature until similar values to those of 5Ru/CeO_2 at 300 °C, and Ru^{n+}-carbonyls intensity of 3Ru/CeO_2 overcomes that of 5Ru/CeO_2 at this temperature. This behaviour indicates that dissociation of the CO_2 molecules is more favourable on 5Ru/CeO_2 at low temperature, which can be attributed to the higher Ru loading, while at high temperature (300 °C) 3Ru/CeO_2 behaves equal for Ru_x-carbonyls and better for Ru^{n+}-carbonyls. The highest concentration of Ru^{n+}-carbonyls formed on 3Ru/CeO_2 at 300 °C is consistent with the highest percentage of Ru^{n+}-CeO_2 species detected

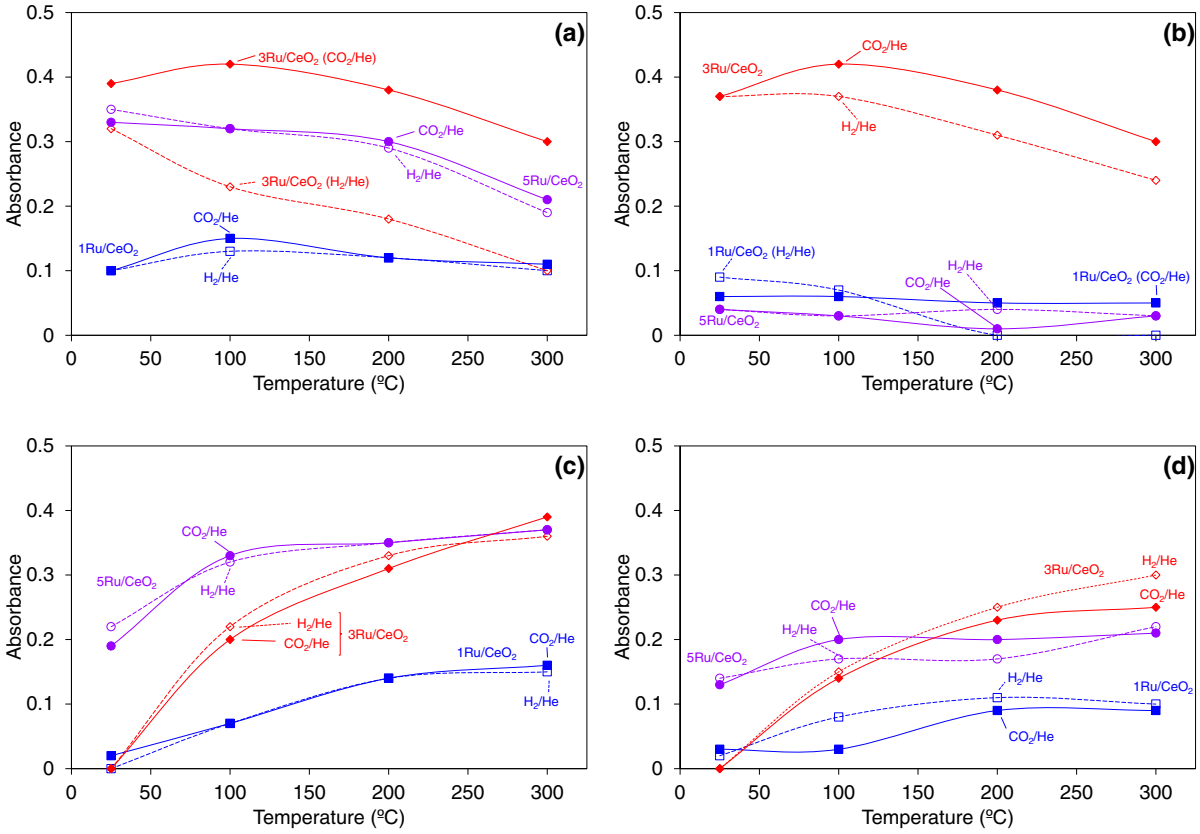

Fig. 8. Intensity of selected infrared bands as a function of temperature. (a) 1615 cm^{-1} (formates), (b) 1280 cm^{-1} (bidentate carbonates), (c) 2030 cm^{-1} (Ru_x-carbonyls) and (d) 1920 cm^{-1} (Ru^{n+}-carbonyls).

by XPS (Table 3), that is, $3Ru/CeO_2$ is the most efficient catalyst for CO_2 dissociation at CO_2 methanation temperatures.

In conclusion, these DRIFTS experiments suggest that the ruthenium loading affects both the chemisorption of CO_2 and the hydrogenation of the surface carbon intermediates. The optimum behaviour is obtained with $3Ru/CeO_2$, which combines good CO_2 chemisorption and dissociation capacity with efficient hydrogenation. CO_2 chemisorption is not very relevant for the lowest ruthenium loading catalyst ($1Ru/CeO_2$), while for the highest ruthenium loading catalyst $5Ru/CeO_2$, hydrogenation is less favourable. According to H_2-TPR and XPS characterization, the optimum behaviour of $3Ru/CeO_2$ could be related to and optimum Ru^{n+}-CeO_2 interaction and formation of a high proportion of highly reducible surface species.

4. Conclusions

The effect of Ru loading on Ru/CeO_2 catalysts has been investigated for the CO_2 methanation reaction, and after screening the 1-5 wt. % range, an optimum loading of 2.5 wt. Ru % has been found. The real amount of Ru determined by ICP is slightly lower to the target value for all Ru/CeO_2 catalysts prepared, since volatile ruthenium oxides are released during the preparation thermal treatment even under inert atmosphere.

The most active Ru/CeO_2 catalyst (with 2.5 wt.% Ru) is the catalyst where ruthenium cations are reduced at the lowest temperature in H_2-TPR experiments (even at room temperature), and is also the catalyst with the highest proportion of ruthenium cations with strong interaction with ceria, as deduced from XPS. XRD characterization suggests partial insertion of ruthenium cations into the ceria lattice.

In situ DRIFTS experiments evidenced that the ruthenium loading affects the chemisorption and dissociation of CO_2 and the hydrogenation of the surface carbon intermediates. The Ru/CeO_2 catalyst with the optimum behaviour (with 2.5 wt. % Ru) combines good CO_2 chemisorption and dissociation capacity with efficient further hydrogenation of the surface carbon intermediates. CO_2 chemisorption was not very relevant for a low ruthenium loading catalyst ($1\%Ru/CeO_2$), while for higher ruthenium loading hydrogenation is less favourable.

Authors' statement

This article has been carried out with equal contribution of all authors.

Declaration of Competing Interest

The authors declare that they have no known competing financial interests or personal relationships that could have appeared to influence the work reported in this paper.

Acknowledgement

Generalitat Valenciana (PROMETEO/2018/0765); MICINN (PID2019-105960RB-C22); Junta de Andalucía (Project P18-RTJ-2974); European Union's Horizon 2020 research and innovation program (Marie Skłodowska-Curie grant agreement No 713567); Science Foundation Ireland Research Centre (award 12/RC/2278_P2).

References

[1] Administration, U. S. E. I. International energy outlook with projections to 2050 *Choice reviews online* 2019.
[2] International Energy Agency (IEA), world energy outlook 2019-Analysis IEA, World energy outlook (2019).
[3] J. Tollefson, COVID curbed carbon emissions in 2020 — but not by much, Nature 589 (7842) (2021) 343.

[4] P. Friedlingstein, M. O'Sullivan, M.W. Jones, R.M. Andrew, J. Hauck, A. Olsen, G. P. Peters, W. Peters, J. Pongratz, S. Sitch, C. le Quéré, J.G. Canadell, P. Ciais, R. B. Jackson, S. Alin, L.E.O.C. Aragão, A. Arneth, V. Arora, N.R. Bates, M. Becker, A. Benoit-Cattin, H.C. Bittig, L. Bopp, S. Bultan, N. Chandra, F. Chevallier, L. P. Chini, W. Evans, L. Florentie, P.M. Forster, T. Gasser, M. Gehlen, D. Gilfillan, T. Gkritzalis, L. Gregor, N. Gruber, I. Harris, K. Hartung, V. Haverd, R.A. Houghton, T. Ilyina, A.K. Jain, E. Joetzjer, K. Kadono, E. Kato, V. Kitidis, J.I. Korsbakken, P. Landschützer, N. Lefèvre, A. Lenton, S. Lienert, Z. Liu, D. Lombardozzi, G. Marland, N. Metzl, D.R. Munro, J.E.M.S. Nabel, S.I. Nakaoka, Y. Niwa, K. O'Brien, T. Ono, P.I. Palmer, D. Pierrot, B. Poulter, L. Resplandy, E. Robertson, C. Rödenbeck, J. Schwinger, R. Séférian, I. Skjelvan, A.J.P. Smith, A.J. Sutton, T. Tanhua, P.P. Tans, H. Tian, B. Tilbrook, G. van der Werf, N. Vuichard, A. P. Walker, R. Wanninkhof, A.J. Watson, D. Willis, A.J. Wiltshire, W. Yuan, X. Yue, S. Zaehle, Global Carbon Budget 2020, Earth Syst. Sci. Data 12 (4) (2020) 3269–3340.

[5] A. Bogaerts, A. Berthelot, S. Heijkers, S. Kolev, R. Snoeckx, S. Sun, G. Trenchev, K. van Laer, W. Wang, CO_2 conversion by plasma technology: insights from modeling the plasma chemistry and plasma reactor design, Plasma Sources Sci. Technol. 26 (6) (2017), 063001.

[6] Y. Zheng, W. Zhang, Y. Li, J. Chen, B. Yu, J. Wang, L. Zhang, J. Zhang, Energy related CO_2 conversion and utilization: advanced materials/nanomaterials, reaction mechanisms and technologies, Nano Energy 40 (2017) 512–539.

[7] R. Snoeckx, A. Bogaerts, Plasma technology – a novel solution for CO_2 conversion? Chem. Soc. Rev. 46 (19) (2017) 5805–5863.

[8] Global CCS Institute (GCI), Global Status of CCS. Global Status of CCS, Global CCS Institute, 2020.

[9] S. Budinis, S. Krevor, Mac Dowell, N. Brandon, A. Hawkes, An assessment of CCS costs, barriers and potential, Energy Strat. Rev. 22 (2018) 61–81.

[10] A. Kätelhön, R. Meys, S. Deutz, S. Suh, A. Bardow, Climate change mitigation potential of carbon capture and utilization in the chemical industry, Proc. Natl. Acad. Sci. 116 (23) (2019) 11187–11194.

[11] L.J. Müller, A. Kätelhön, M. Bachmann, A. Zimmermann, A. Sternberg, A. Bardow, A guideline for life cycle assessment of carbon capture and utilization, Front. Energy Res. 8 (2020) 15.

[12] A. Sápi, T. Rajkumar, M. Ábel, A. Efremova, A. Grósz, A. Gyuris, K.B. Ábrahámné, I. Szenti, J. Kiss, T. Varga, Á. Kukovecz, Z. Kónya, Noble-metal-free and pt nanoparticles-loaded, mesoporous oxides as efficient catalysts for CO_2 hydrogenation and dry reforming with methane, J. CO_2 Util. 32 (2019) 106–118.

[13] A. Sápi, G. Halasi, J. Kiss, D.G. Dobó, K.L. Juhász, V.J. Kolcsár, Z. Ferencz, G. Vári, V. Matolin, A. Erdőhelyi, Á. Kukovecz, Z. Kónya, In situ DRIFTS and NAP-XPS exploration of the complexity of CO_2 hydrogenation over size-controlled Pt nanoparticles supported on mesoporous NiO, J. Phys. Chem. C 122 (10) (2018) 5553–5565.

[14] A.H. Zamani, R. Ali, W.A.W. Abu Bakar, Optimization of CO_2 methanation reaction over M*/Mn/Cu–Al_2O_3 (M*: Pd, Rh and Ru) catalysts, J. Ind. Eng. Chem. 29 (2015) 238–248.

[15] K. Chang, H. Zhang, M. Cheng, Q. Lu, Application of ceria in CO_2 conversion catalysis, ACS Catal. 10 (1) (2020) 613–631.

[16] A. Trovarelli, Catalytic properties of ceria and CeO_2-containing materials, Catal. Rev. 38 (4) (1996) 439–520.

[17] S. Letichevsky, C.A. Tellez, R.R. de Avillez, M.I.P. da Silva, M.A. Fraga, L.G. Appel, Obtaining CeO_2–ZrO_2 mixed oxides by coprecipitation: role of preparation conditions, Appl. Catal. B 58 (3–4) (2005) 203–210.

[18] F. Wang, M. Wei, D.G. Evans, X. Duan, CeO_2-based heterogeneous catalysts toward catalytic conversion of CO_2, J. Mater. Chem. A 4 (16) (2016) 5773–5783.

[19] R.X. Valenzuela, G. Bueno, V. Cortés Corberán, Y. Xu, C. Chen, Selective oxidehydrogenation of ethane with CO_2 over CeO_2-based catalysts, Catal. Today 61 (1–4) (2000) 43–48.

[20] R. di Monte, J. Kašpar, Heterogeneous environmental catalysis – a gentle art: CeO_2–ZrO_2 mixed oxides as a case history, Catal. Today 100 (1–2) (2005) 27–35.

[21] Y. Guo, S. Mei, K. Yuan, D.J. Wang, H.C. Liu, C.H. Yan, Y.W. Zhang, Low-temperature CO_2 methanation over CeO_2-supported ru single atoms, nanoclusters, and nanoparticles competitively tuned by strong metal-support interactions and H-spillover effect, ACS Catal. 8 (7) (2018) 6203–6215.

[22] J.A.H. Dreyer, P. Li, L. Zhang, G.K. Beh, R. Zhang, P.H.-L. Sit, W.Y. Teoh, Influence of the oxide support reducibility on the CO_2 methanation over Ru-based catalysts, Appl. Catal. B 219 (2017) 715–726.

[23] S. Kattel, P. Liu, J.G. Chen, Tuning selectivity of CO_2 hydrogenation reactions at the metal/oxide interface, J. Am. Chem. Soc. 139 (29) (2017) 9739–9754.

[24] W. Wang, Z. Qu, L. Song, Q. Fu, CO_2 hydrogenation to methanol over Cu/CeO_2 and Cu/ZrO_2 catalysts: tuning methanol selectivity via metal-support interaction, J. Energy Chem. 40 (2020) 22–30.

[25] X.I. Pereira-Hernández, A. DeLaRiva, V. Muravev, D. Kunwar, H. Xiong, B. Sudduth, M. Engelhard, L. Kovarik, E.J.M. Hensen, Y. Wang, A.K. Datye, Tuning Pt-CeO_2 interactions by high-temperature vapor-phase synthesis for improved reducibility of lattice oxygen, Nat. Commun. 10 (1) (2019) 1358.

[26] Z. Xiao, X. Zhang, F. Hou, C. Wu, L. Wang, G. Li, Tuning metal-support interaction and oxygen vacancies of ceria supported nickel catalysts by Tb doping for n-dodecane steam reforming, Appl. Surf. Sci. 503 (2020), 144319.

[27] S. Tada, T. Shimizu, H. Kameyama, T. Haneda, R. Kikuchi, Ni/CeO_2 catalysts with high CO_2 methanation activity and high CH_4 selectivity at low temperatures, Int. J. Hydrogen Energy 37 (7) (2012) 5527–5531.

[28] Z. Bian, Y.M. Chan, Y. Yu, S. Kawi, Morphology dependence of catalytic properties of Ni/CeO_2 for CO_2 methanation: a kinetic and mechanism study, Catal. Today 347 (2018) 31–38.

[29] A. Cárdenas-Arenas, A. Quindimil, A. Davó-Quiñonero, E. Bailón-García, D. Lozano-Castelló, U. De-La-Torre, B. Pereda-Ayo, J.A. González-Marcos, J. R. González-Velasco, A. Bueno-López, Isotopic and in situ DRIFTS study of the CO_2 methanation mechanism using Ni/CeO_2 and Ni/Al_2O_3 catalysts, Appl. Catal. B 265 (2020), 118538.

[30] L.R. Winter, R. Chen, X. Chen, K. Chang, Z. Liu, S.D. Senanayake, A.M. Ebrahim, J. G. Chen, Elucidating the roles of metallic Ni and oxygen vacancies in CO_2 hydrogenation over Ni/CeO_2 using isotope exchange and in situ measurements, Appl. Catal. B 245 (2019) 360–366.

[31] N. Rui, X. Zhang, F. Zhang, Z. Liu, X. Cao, Z. Xie, R. Zou, S.D. Senanayake, Y. Yang, J.A. Rodriguez, C.J. Liu, Highly active Ni/CeO_2 catalyst for CO_2 methanation: preparation and characterization, Appl. Catal. B 282 (2021), 119581.

[32] B. Wang, Y. Xiong, Y. Han, J. Hong, Y. Zhang, J. Li, F. Jing, W. Chu, Preparation of stable and highly active Ni/CeO_2 catalysts by glow discharge plasma technique for glycerol steam reforming, Appl. Catal. B 249 (2019) 257–265.

[33] T.S. Galhardo, A.H. Braga, B.H. Arpini, J. Szanyi, R.v. Gonçalves, B.F. Zornio, C. R. Miranda, L.M. Rossi, Optimizing active sites for high CO selectivity during CO_2 hydrogenation over supported nickel catalysts, J. Am. Chem. Soc. 143 (11) (2021) 4268–4280.

[34] J. Li, Y. Lin, X. Pan, D. Miao, D. Ding, Y. Cui, J. Dong, X. Bao, Enhanced CO_2 methanation activity of Ni/anatase catalyst by tuning strong metal-support interactions, ACS Catal. 9 (7) (2019) 6342–6348.

[35] G.N. Vayssilov, Y. Lykhach, A. Migani, T. Staudt, G.P. Petrova, N. Tsud, T. Skála, A. Bruix, F. Illas, K.C. Prince, V. Matolín, K.M. Neyman, J. Libuda, Support nanostructure boosts oxygen transfer to catalytically active platinum nanoparticles, Nat. Mater. 10 (4) (2011) 310–315.

[36] K. Liu, R. Qin, N. Zheng, Insights into the interfacial effects in heterogeneous metal nanocatalysts toward selective hydrogenation, J. Am. Chem. Soc. 143 (12) (2021) 4483–4499.

[37] S.J. Tauster, S.C. Fung, R.T.K. Baker, J.A. Horsley, Strong interactions in supported-metal catalysts, Science 211 (4487) (1981) 1121–1125.

[38] B. Han, Y. Guo, Y. Huang, W. Xi, J. Xu, J. Luo, H. Qi, Y. Ren, X. Liu, B. Qiao, T. Zhang, Strong metal–support interactions between Pt single atoms and TiO_2, Angew. Chem. Int. Ed. 59 (29) (2020) 11824–11829.

[39] S.J. Tauster, S.C. Fung, R.L. Garten, Strong metal-support interactions. Group 8 noble metals supported on titanium dioxide, J. Am. Chem. Soc. 100 (1) (1978) 170–175.

[40] B. Miao, S.S.K. Ma, X. Wang, H. Su, S.H. Chan, Catalysis mechanisms of CO_2 and CO methanation, Catal. Sci. Technol. 6 (12) (2016) 4048–4058.

[41] S.-T. Zhang, H. Yan, M. Wei, D.G. Evans, X. Duan, Hydrogenation mechanism of carbon dioxide and carbon monoxide on Ru(0001) surface: a density functional theory study, RSC Adv. 4 (57) (2014) 30241–30249.

[42] P. Panagiotopoulou, D.I. Kondarides, X.E. Verykios, Mechanistic study of the selective methanation of CO over Ru/TiO_2 catalyst: identification of active surface species and reaction pathways, J. Phys. Chem. C 115 (4) (2011) 1220–1230.

[43] K. Zhao, L. Wang, M. Calizzi, E. Moioli, A. Züttel, In situ control of the adsorption species in CO_2 hydrogenation: determination of intermediates and byproducts, J. Phys. Chem. C 122 (36) (2018) 20888–20893.

[44] G.D. Weatherbee, C.H. Bartholomew, Hydrogenation of CO_2 on group VIII metals: II. Kinetics and mechanism of CO_2 hydrogenation on nickel, J. Catal. 77 (2) (1982) 460–472.

[45] A. Karelovic, P. Ruiz, Mechanistic study of low temperature CO_2 methanation over Rh/TiO_2 catalysts, J. Catal. 301 (2013) 141–153.

[46] F. Wang, S. He, H. Chen, B. Wang, L. Zheng, M. Wei, D.G. Evans, X. Duan, Active site dependent reaction mechanism over Ru/CeO_2 catalyst toward CO_2 methanation, J. Am. Chem. Soc. 138 (19) (2016) 6298–6305.

[47] C. Vogt, M. Monai, E.B. Sterk, J. Palle, A.E.M. Melcherts, B. Zijlstra, E. Groeneveld, P.H. Berben, J.M. Boereboom, E.J.M. Hensen, F. Meirer, I.A.W. Filot, B. M. Weckhuysen, Understanding carbon dioxide activation and carbon–carbon coupling over nickel, Nat. Commun. 10 (1) (2019) 5330.

[48] A. Aitbekova, L. Wu, C.J. Wrasman, A. Boubnov, A.S. Hoffman, E.D. Goodman, S. R. Bare, M. Cargnello, Low-temperature restructuring of CeO_2-supported Ru nanoparticles determines selectivity in CO_2 catalytic reduction, J. Am. Chem. Soc. 140 (42) (2018) 13736–13745.

[49] K. He, N. Chen, C. Wang, L. Wei, J. Chen, Method for determining crystal grain size by X-ray diffraction, Cryst. Res. Technol. 53 (2) (2018), 1700157.

[50] S. Sharma, Z. Hu, P. Zhang, E.W. McFarland, H. Metiu, CO_2 methanation on Ru-doped ceria, J. Catal. 278 (2018) 297–309.

[51] S. Sharma, K.B.S. Kumar, Y.M. Chandnani, V.S.P. Kumar, B.P. Gangwar, A. Singhal, P.A. Deshpande, Mechanistic insights into CO_2 methanation over Ru-substituted CeO_2, J. Phys. Chem. C 120 (2016) 14101–14112.

[52] T. Sakpal, L. Lefferts, Structure-dependent activity of CeO_2 supported Ru catalysts for CO_2 methanation, J. Catal. 367 (2018) 171–180.

[53] H.T.T. Nguyen, Y. Kumabe, S. Ueda, K. Kan, M. Ohtani, K. Kobiro, Highly durable Ru catalysts supported on CeO_2 nanocomposites for CO_2 methanation, Appl. Catal. A Gen. 577 (2019) 35–43.

[54] J.S.J. Hargreaves, Some considerations related to the use of the scherrer equation in powder X-ray diffraction as applied to heterogeneous catalysts, Catal. Struct. React. 2 (1–4) (2016) 33–37.

[55] N. Guillén-Hurtado, J. Giménez-Mañogil, J.C. Martínez-Munuera, A. Bueno-López, A. García-García, Study of Ce/Pr ratio in ceria-praseodymia catalysts for soot combustion under different atmospheres, Appl. Catal. A 590 (2020), 117339.

[56] I. Atribak, A. Bueno-López, A. García-García, Role of yttrium loading in the physico-chemical properties and soot combustion activity of ceria and ceria–zirconia catalysts, J. Mol. Catal. A 300 (1) (2009) 103–110.

[57] S. Eckle, H.G. Anfang, R.J. Behm, Reaction intermediates and side products in the methanation of CO and CO_2 over supported Ru catalysts in H2-rich reformate gases, J. Phys. Chem. C 115 (4) (2011) 1361–1367.
[58] H.S. Gandhi, G.W. Graham, R.W. McCabe, Automotive exhaust catalysis, J. Catal. 216 (2003) 433–442.
[59] N. Labhsetwar, A. Watanabe, S. Rayalu, J. Subrt, T. Mistuhashi, S. Devotta, H. Haneda, Catalytic properties of strontium ruthenate perovskite prepared by hot isostatic pressure method, In, Stud. Surf. Sci. Catal. 162 (2006) 825–831.
[60] A. Porta, L. Falbo, C.G. Visconti, L. Lietti, C. Bassano, P. Deiana, Synthesis of Ru-based catalysts for CO_2 methanation and experimental assessment of intraporous transport limitations, Catal. Today 343 (2020) 38–47.
[61] S. Navarro-Jaén, J.C. Navarro, L.F. Bobadilla, M.A. Centeno, O.H. Laguna, J. A. Odriozola, Size-tailored Ru nanoparticles deposited over γ-Al_2O_3 for the CO_2 methanation reaction, Appl. Surf. Sci. 483 (2019) 750–761.
[62] S. Hosokawa, State of Ru on CeO_2 and its catalytic activity in the wet oxidation of acetic acid, Appl. Catal. B 45 (3) (2003) 181–187.
[63] L. He, Y. Ren, Y. Fu, B. Yue, S. Tsang, H. He, Morphology-dependent catalytic activity of Ru/CeO_2 in dry reforming of methane, Molecules 24 (3) (2019) 526.
[64] T. Sakpal, L. Lefferts, Structure-dependent activity of CeO_2 supported Ru catalysts for CO_2 methanation, J. Catal. 367 (2018) 171–180.
[65] D.J. Morgan, Resolving ruthenium: XPS studies of common ruthenium materials, Surf. Interface Anal. 47 (11) (2015) 1072–1079.
[66] Y. Hartadi, D. Widmann, R.J. Behm, Methanol formation by CO_2 hydrogenation on Au/ZnO catalysts – effect of total pressure and influence of CO on the reaction characteristics, J. Catal. 333 (2016) 238–250.